

Loss of ABCA8B decreases myelination by reducing oligodendrocyte precursor cells in mice

Yiran Liu^{1,2,3,*}, David Castano^{1,2,3,*}, Francesco Girolamo⁴, Laia Trigueros-Motos¹, Han-Gyu Bae⁵, Suat Peng Neo⁶, Jeongah Oh⁷, Pradeep Narayanaswamy⁷, Federico Torta⁷, Kerry Anne Rye⁸, Dong-Gyu Jo⁹, Jayantha Gunaratne⁶, Sangyong Jung⁵, Daniela Virgintino⁴, and Roshni R. Singaraja^{1,2,3,*}

¹Translational Laboratories in Genetic Medicine, Agency for Science, Technology and Research, Singapore, Singapore;

²Department of Medicine, Yong Loo Lin School of Medicine, National University of Singapore, Singapore, Singapore;

³Cardiovascular Research Institute, National University Health System, Singapore, Singapore; ⁴Department of Basic Medical Sciences, Neurosciences, and Sensory Organs, Human Anatomy and Histology Unit, University of Bari School of Medicine, Bari, Italy; ⁵Singapore Bioimaging Consortium, and ⁶Institute of Molecular and Cell Biology, Agency for Science, Technology and Research, Singapore, Singapore; ⁷Singapore Lipidomics Incubator, Department of Biochemistry, Life Sciences Institute and Yong Loo Lin School of Medicine, National University of Singapore, Singapore, Singapore; ⁸School of Medical Sciences, University of New South Wales, Sydney, Australia; ⁹School of Pharmacy, Sungkyunkwan University, Suwon, Korea

Abstract The myelin sheath, which is wrapped around axons, is a lipid-enriched structure produced by mature oligodendrocytes. Disruption of the myelin sheath is observed in several neurological diseases, such as multiple sclerosis. A crucial component of myelin is sphingomyelin, levels of which can be increased by ABCA8, a member of the ATP-binding cassette transporter family. ABCA8 is highly expressed in the cerebellum, specifically in oligodendroglia. However, whether ABCA8 plays a role in myelination and mechanisms that would underlie this role remain unknown. Here, we found that the absence of *Abca8b*, a mouse ortholog of *ABCA8*, led to decreased numbers of cerebellar oligodendrocyte precursor cells (OPCs) and mature oligodendrocytes in mice. We show that in oligodendrocytes, ABCA8 interacts with chondroitin sulfate proteoglycan 4 (CSPG4), a molecule essential for OPC proliferation, migration, and myelination. In the absence of *Abca8b*, localization of CSPG4 to the plasma membrane was decreased, contributing to reduced cerebellar CSPG4 expression. Cerebellar CSPG4+ OPCs were also diminished, leading to decreased mature myelinating oligodendrocyte numbers and cerebellar myelination levels in *Abca8b*^{-/-} mice. In addition, electron microscopy analyses showed that the number of nonmyelinated cerebellar axons was increased, whereas cerebellar myelin thickness (g-ratio), myelin sheath periodicity, and axonal diameter were all decreased, indicative of disordered myelin ultrastructure. In line with disrupted cerebellar myelination, *Abca8b*^{-/-} mice showed lower cerebellar conduction velocity and disturbed locomotion. In summary, ABCA8 modulates cerebellar myelination, in part through functional regulation of the ABCA8-interacting protein CSPG4. Our findings suggest that ABCA8

disruption may contribute to the pathophysiology of myelin disorders.

Supplementary key words hypomyelination • ABCA8 • cerebellum • animal models • brain lipids • lipid transfer proteins • cholesterol/trafficking • CSPG4 • myelin disorders • myelin sheath periodicity

ABCA8 belongs to the ABC family whose members are involved in the ATP-dependent transport of various substrates, such as metabolic products, ions, drugs, peptides, and lipids, across membranes (1). The ABCA subclass consists of transmembrane transporters of endogenous lipids, and some members contribute to brain lipid transport and myelination (2, 3). ABCA1, a key regulator of cholesterol efflux, lipidates apolipoprotein E (apoE) particles that are secreted from astrocytes and microglia (4). These sparsely lipidated particles are suggested to take up additional lipids, likely via other ABC transporters, forming more mature particles that bind amyloid β and enable its clearance through apoE receptors (2, 5). Brain-specific *Abca1*^{-/-} mice exhibit reduced myelinated axons and decreased thickness of their myelin sheaths (6). ABCA2 shows highest expression in oligodendrocytes and Schwann cells in the CNS and peripheral nervous system (PNS) and is thought to play a role in myelin lipid transport (2). In *Abca2*^{-/-} mice, spinal cord myelin sheath thickness was increased, whereas both spinal cord and cerebral myelin membrane periodicity and sphingomyelin levels were reduced (7, 8). ABCA7 increased cholesterol efflux to discoidal apoE-containing particles (9), suggesting that ABCA7 also facilitates lipid transport in the brain. ABCA7 appears to be a risk factor for Alzheimer's disease (AD) (10), and

*These authors contributed equally to the manuscript.

*For correspondence: Roshni R. Singaraja, mdcrs@nus.edu.sg.

sphingomyelin, a myelin-enriched lipid, was significantly decreased in brains of *Abca7* null mice (11).

ABCA8 was originally cloned as a gene with unknown function from human brain libraries (3). We identified mutations in *ABCA8* as underlying reduced serum HDL-C levels in humans and found that ABCA8 facilitated the efflux of cholesterol to lipid-free APOA-I, thus increasing HDL-C levels (12). The human *ABCA8* gene has two mouse orthologs, *Abca8a* and *Abca8b*. In line with a role for human ABCA8 in HDL-C metabolism, *Abca8b*^{-/-} mice showed reduced plasma HDL-C levels (12), further confirming a role for ABCA8 in lipid transport.

In the brain, ABCA8 showed highest expression in the superior frontal and inferior temporal white matter, indicating possible functional importance for ABCA8 specific to white matter (13). Sphingomyelin is a sphingolipid found in myelin sheaths (14). ABCA8 was shown to increase sphingomyelin production by increasing the expression of the sphingomyelin synthesis gene *sphingomyelin synthase 1* (*SGMS1*) in vitro (13), suggesting a role for ABCA8 in myelination in the CNS. However, ABCA8 belongs to the ABC family of transporters, not known for their function as transcriptional regulators, suggesting that the role for ABCA8 in the brain remains unclear.

The *ABCA8* gene has been linked to susceptibility loci for multiple sclerosis (15), an autoimmune disease of CNS myelin, frequently affecting the cerebellum (16). As well, the *ABCA8* transcript is significantly increased in Huntington disease (16), multiple systems atrophy (17), epilepsy (18), and during ageing (19), all of which are associated with dysfunctional white matter (20–23). *ABCA8* has also been suggested to act as an oligodendrocyte differentiation regulator as its expression was upregulated during induced proliferation and differentiation of oligodendrocyte precursor cells (OPCs) (15, 24).

Together, these findings suggest a role for ABCA8 in myelination in the CNS. However, a direct role for ABCA8 in the modulation of myelin has not yet emerged. Here, we find that myelination in the CNS is reduced in the absence of *Abca8b*, modulated in part by altered function of the ABCA8-interacting protein chondroitin sulfate proteoglycan 4 (*Cspg4*), a gene essential for regulating OPC proliferation and migration, as well as oligodendrocyte numbers, thus modulating myelination.

MATERIALS AND METHODS

Mice

Sperm were obtained from the Knockout Mouse Project Repository (UC-Davis KOMP Repository) from mice in which exon 3 of *Abca8b* was flanked with *Frt* and *LoxP* DNA cleavage sites. Homozygous *Flp-recombinase* mice from the Jackson Laboratory (Bar Harbor, ME) were first crossed with *Abca8bFlpCre* mice to obtain *FlpAbca8b* mice with Flp recognition target-

mediated cleavage of the promoter cassette. Homozygous whole-body *Cre-recombinase* mice from the Jackson Laboratory were then crossed to these mice to obtain *CreFlpAbca8b* mice with loxP-mediated cleavage of exon 3. The removal of exon 3 creates an in-frame stop codon within the protein sequence leading to the truncation of the *Abca8b* protein. Mice were generated on the *C57BL6/J* background.

Genotypes were determined by PCR as described (12). All experiments used male mice that were provided standard chow diet (1324_u modified; Altromin GmbH & Co, Germany) and water ad libitum and maintained under a 12 h light/dark cycle. All animal experiments were approved by the Biomedical Sciences Institute Singapore Institutional Animal Care Committee.

Gene expression analyses

Brain RNA was extracted using the RNeasy Mini Kit (Qiagen), and complementary DNA (cDNA) was synthesized using SuperScript II Reverse Transcriptase (Invitrogen, Carlsbad, CA). Primer sequences are indicated in supplemental Table S1. Relative expressions were calculated according to the formula $2^{(-\Delta\Delta Ct)}$, and the results are expressed as average gene expression \pm SEM, using *Rpl37* as control.

Black-Gold II myelin staining

Sagittal cryosections from postnatal day 20 mice were mounted onto gelatin-coated slides and air dried. Slides were then rehydrated, transferred to a 0.3% Black-Gold II solution dissolved in 0.9% saline (Black-Gold II Myelin Staining Kit; EMD Millipore), and heated to 65°C. The extent of stain impregnation was monitored microscopically. Slides were rinsed, transferred to 1% sodium thiosulfate for 3 min, rinsed again, and then dehydrated via graduated alcohol solutions (70%, 95%, and 100% ethanol). Slides were immersed in xylene and mounted with DPX (Sigma-Aldrich, MO). Images were obtained with a Nikon Ni-E microscope equipped with a Nikon DS-Ri2 camera and analyzed using Nikon NIE-Elements software (Tokyo, Japan) at the Singapore Bio-imaging Consortium (SBIC).

Electron microscopy and analyses

Mice were transcardially perfused with 4% paraformaldehyde (PFA)/2% glutaraldehyde (pH 7.4), brains were isolated and postfixed overnight at 4°C in the same buffer, and washed in PBS. Brains were sent to the Scanning Electron Microscopy unit, Sunkyunkwan University, Korea, for processing and imaging. Myelinated and nonmyelinated axons were counted in five random images of 100 μm^2 in five mice/genotype. G-ratios were calculated as the diameter of the axons divided by the diameter of the axons and the surrounding myelin sheaths in a total of 800 axons/genotype. Myelin thickness was calculated by measuring the outer diameter in 800 axons from five mice/genotype. Periodicity was calculated by dividing myelin thickness (in nanometers) by the number of myelin sheets in 80 axons per genotype.

Cerebellar compound action potential recording

The cerebella were extracted from mice and sliced horizontally (transverse) at 450 μm thickness in ice-cold oxygenated artificial cerebrospinal fluid (in millimolars: 216 sucrose, 2 KCl, 1.25 NaH_2PO_4 , 26 NaHCO_3 , 10 glucose, 2 MgCl_2 , 2

MgSO₄, and 1 CaCl₂) with a vibratome (VT1200s; Leica, Nussloch, Germany). The cerebellar slices were immediately transferred to prewarmed oxygenated artificial cerebrospinal fluid (34°C, in millimeter; 124 NaCl, 2.5 KCl, 1.2 NaH₂PO₄, 24 NaHCO₃, 5 HEPES, 12.5 glucose, 2 MgSO₄, and 2 CaCl₂), warmed to 34°C, recovered for 30 min, and placed at room temperature until use. Compound action potentials after 0.5 ms of stimuli (3 mA) applied by a stimulator (Model 2100; A-M Systems, Sequim, WA) were measured in cerebellar parallel fibers using MultiClamp 700A and digitized using DigiData 1550B (Axon Instruments, San Jose, CA). Responses were measured 0.5 and 1.0 mm away from the stimulating electrode. Each recording was performed in triplicate, and the averaged peak latencies were used to compare the conduction velocity between groups.

Gait analyses

Gait analyses were performed on 6-week-old male mice using an adapted runway system (25). To obtain footprints, the forefeet and hindfeet were painted with red and black nontoxic water-based paint, respectively. Mice were allowed to walk on a strip of paper along a custom-made 50 cm long, 13 cm wide, and 10 cm high tunnel with a darkened goal chamber at one end. Each mouse had three runs, and only clear and nonsmudged footprints (excluding the first and last footprints) were analyzed. Stride length was measured as the distance between two sequential footprints created by the same foot. Stride width was measured as the distance between the left and right forelimbs or hind limbs (25). Toe spread was measured as the distance between the first and the fifth toes. Each set of measurements was averaged to obtain these parameters per mouse.

Construct and lentiviral production

pcDNA-ABCA8-v5 was obtained as previously described (12), N-terminally tagged with the myc-BirA* biotinylation enzyme, and cloned into the *pTRIPZ* lentiviral vector (OpenBiosystem, Singapore). Lentivirus particles were generated according to the manufacturer's protocol (OpenBiosystem), and 293T cells (ATCC, Manassas, VA) were infected using standard procedures (26).

BirA*-fusion proteins, biotinylation, and affinity capture of biotinylated proteins

Human glial (oligodendrocytic) hybrid cell line (MO3.13; Cedarlane, ON, Canada) stably expressing myc-BirA-ABCA8-v5 was generated by lentiviral transduction and selected with 1.0 µg/ml puromycin. The myc-BirA*-fusion construct was expressed upon induction with doxycycline for at least 6 days prior to analysis. Induction was verified by Western blotting using an anti-myc antibody (sc40; Santa Cruz, Dallas, TX). 50 µM biotin was added to the medium for 24 h prior to cell lysis under denaturing conditions (M-lysis buffer; Roche, Basel, Switzerland). Control cells not induced with doxycycline or without addition of biotin were processed in parallel. Biotinylated proteins were purified using streptavidin-coupled magnetic beads (Invitrogen). After reduction and alkylation, purified proteins were separated by 4–12% NuPage Novex Bis-Tris gels (Invitrogen), stained with Colloidal Blue (Invitrogen), and digested in-gel using trypsin (27).

Mass spectrometry and data analyses

Tryptic peptides were analyzed using Thermo Scientific Easy-nLC with a 15 cm column (Acclaim PepMap™ RSLC; C18, 100 Å, 2 µm, 7.5 × 15 cm) coupled with Orbitrap classic (Thermo Fisher Scientific). Peptides were loaded with 0.1% formic acid, 2% acetonitrile, and eluted with a 120 min gradient at 250 nl/min with 8–38% buffer B (0.1% formic acid and 80% acetonitrile). Mass spectra were acquired in positive ion mode. Survey full scan MS spectra (*m/z* 310–1,400) were acquired with a resolution of *r* = 60,000 and an automatic gain control target of 1 × 10⁶. The 10 most intense peptide ions in each scan with ion intensity of >2,000 counts and charge state ≥2 were isolated sequentially to a target value of 1 × 10⁴ and fragmented in the linear ion trap by collision-induced dissociation using normalized collision energy of 35%. A dynamic exclusion was applied using a maximum exclusion list of 500 with one repeat and an exclusion duration of 30 s. All samples were analyzed using Mascot 2.4.1 (Matrix Science, London, UK), which searched against 160,615_human_database selected for Homo sapiens from UniProt of 154,434 entries. Mascot was searched with a fragment ion mass tolerance of 0.50 Da and a parent ion tolerance of 6.0 ppm. Carbamidomethyl of cysteine was specified as a fixed modification, and oxidation of methionine and acetyl of the N terminus were specified as variable modifications in Mascot. The .dat outputs from Mascot were merged using Scaffold (Scaffold_4.9.0; Proteome Software, Inc, Portland, OR). Peptide identifications were accepted if they were >95.0% probability by the Peptide Prophet algorithm. Protein identifications were accepted if they were >99.0% probability and contained at least two identified peptides. Peptide false discovery rate was 0.1% (decoy), and protein false discovery rate was 0.4% (decoy).

BioID purification and data analysis

Three rounds of BioID were performed, followed by mass spectrometric analyses of peptides. Proteins with a relatively high number of unique peptides identified in the myc-BirA* sample and almost no unique peptides in the negative control samples were defined as strong interacting candidates. Comprehensive lists of target proteins were generated using Scaffold 4.9.0 (Proteome Software, Inc). Diagrams of protein interactions were generated using Cytoscape (version 3.0; National Institute of General Medical Sciences). Proteins with roles in myelination were selected for further studies.

Coimmunoprecipitation assays

pEF6-CSPG4-myc-his plasmid was purchased from Addgene (Cambridge, MA). DNA was ligated into *pcDNA™3.1(+)* (Thermo Fisher Scientific), amplified, and sequence confirmed. Human embryonic kidney 293T cells (ATCC) were cotransfected with human-*V5-ABCA8-pcDNA3.1* and *myc-CSPG4* using Lipofectamine 300 reagent (Thermo Fisher Scientific). Twenty-four hours after transfection, cells were lysed in 10 mM Tris-HCl, 0.1% Triton, 150 mM NaCl, pH 8.0, 1× protease inhibitor cocktail (Roche, Basel, Switzerland), and centrifuged at 14,000 *g* for 20 min at 4°C. Protein A sepharose beads (50 µl; GE Healthcare, MA) were incubated for 2 h at 4°C with 2 µg anti-V5 antibody (Invitrogen) or anti-c-myc antibody 9E10 (Santa Cruz Biotechnology, Dallas, TX). The cell lysates (500 µg) were incubated with the beads overnight at 4°C. Nonspecific binding was assessed using beads incubated without protein lysate. Beads were washed in cold homogenization buffer containing 0.4% Tween-20, and the bound proteins were detached using sample buffer

containing 200 mM dithiothreitol at 100°C for 5 min. Samples were analyzed by Western blotting to detect human ABCA8 (anti-V5 [Invitrogen]) and anti-c-myc antibody (9E10) to detect tagged CSPG4.

OPC analyses

Pups at postnatal days 4, 7, and 9 were anesthetized and transcardially perfused with PBS followed by 4% PFA. Brains were postfixed in 4% PFA for 12 h, followed by immersion in 30% sucrose at 4°C. Brains were then coated in 7.5% gelatin and 15% sucrose in PBS at 4°C overnight. The gelatin blocks were flash frozen for cryosectioning using isopentane and stored at -80°C.

For fluorescent staining, slides containing 20 µm sections were pretreated with 1 N HCl for 15 min, 2 N HCl for 25 min, and neutralized with 0.1 M borate buffer for antigen retrieval. Slides were then blocked in 5% normal goat serum (NGS; Merck, NJ), 0.2% Triton X-100 in PBS, followed by incubation with anti-platelet-derived growth factor receptor alpha antibody (1:500; AF1062; R&D Systems, MN) in PBS with 1% NGS, 0.2% Triton X-100 overnight. Sections were then incubated with donkey anti-goat 555 Alexa Fluor (1:500; Thermo Fisher Scientific) in 0.2% Triton/PBS and mounted in Dako Fluorescent Mounting Medium (Agilent Technologies, CA). Fluorescence images were obtained using a Ti-E (Nikon Instruments, Inc, Tokyo, Japan) microscope equipped with a digital camera (Zyla 4.2 sCMOS; Andor Technology), and analyzed using NIE-Elements software (Nikon Instruments, Inc) at the SBIC.

For CSPG4 analyses, pups at postnatal day 8 were anesthetized and transcardially perfused with 100–150 ml of 2% PFA and 0.2% glutaraldehyde PBS. Whole brains were removed and postfixed by immersion in the same fixative at 4°C for 4 h, washed in PBS overnight at 4°C, and stored in 0.02% PFA in PBS at 4°C. Using a vibrating microtome (Leica Microsystem), serial sagittal hindbrain sections (thickness of 15/20 µm) were cut and collected as free-floating sections in 0.02% PFA in PBS in a multiwell archive at 4°C. Briefly, after permeabilization (0.5% Triton X-100 in PBS), free-floating sections were incubated as follows: anti-CSPG4 (1:180; AB5320; Merck Millipore, Darmstadt, Germany) overnight at 4°C, biotinylated goat antirabbit (1:500; BA1000; Vector Laboratories, Burlingame, CA) for 45 min at room temperature, Streptavidin-Alexa Fluor™ 488 (1:500; Invitrogen), and Alexa Fluor™ 555-conjugated wheat germ agglutinin (WGA-555 W32464; Thermo Fisher Scientific) for 45 min at room temperature, and nuclear TO-PRO-3 (1:10,000; Invitrogen) for 15 min at room temperature. Finally, the sections were collected on Vectabond™-treated slides and coverslipped with Vectashield (both Vector Laboratories). Negative controls were prepared by omitting the primary antibody or WGA and mismatching the secondary antibody. Sections were examined under Leica TCS SP5 confocal laser scanning microscope (Leica Microsystems, Wetzlar, Germany) using a sequential scan procedure. Confocal images were taken at 0.35 µm intervals through the *z*, *x*, and *y*-axes of the section, with 40× and 63× oil lenses.

Quantitative assessment of OPC density was carried out on four sections per brain from *wt* (*n* = 5) and *Abca8b*^{-/-} (*n* = 5) mice by computer-aided morphometric analysis using the Leica Confocal Multicolor Package (Leica Microsystems) and ImageJ (the National Institutes of Health, Bethesda, MD) software. The number of CSPG4⁺ OPCs was interactively counted and reported to the reference volume of 10⁶ µm³; each CSPG4⁺ OPC was allocated in a specific cerebellar lobe

according to the Allen Brain Atlas (<https://mouse.brain-map.org/static/atlas>). Cell size and shape descriptors of OPCs were evaluated by means of Analyze Skeleton (2D/3D) plugin (28), and the obtained binary OPC outlines were morphometrically analyzed by FracLac plugin (<http://rsb.info.nih.gov/ij/plugins/fracLac/FLHelp/Introduction.htm.1999-2013>). The chosen descriptors included the number of OPC process end points, the total branch length per OPC, the index of increasing complexity of cell shape (fractal dimension), and the index of cell shape heterogeneity (lacunarity).

Quantitative evaluation of the colocalization of CSPG4 and WGA-555 fluorescence pixels was performed by two independent observers (D.V. and F.G.), blinded for group allocation, using ImageJ EzColocalization plugin (the National Institutes of Health), according to the developer's instructions (29). Analyses were performed on the cerebellum of *wt* and *Abca8b*^{-/-} mice (*Abca8b*^{+/+}, *n* = 5, and *Abca8b*^{-/-}, *n* = 5). The high magnification power fields, each showing a single OPC, were analyzed using EzColocalization to obtain the Pearson's coefficient (P), Mander's colocalization coefficients M1 (CSPG4 overlapping WGA-555) and M2 (WGA555 overlapping CSPG4), heat maps of threshold overlap score of linear metric matrix, and scatter plots of relationship between the signal intensity for the two channels in each pixel of the images. The mean fluorescence intensity of CSPG4 expression was calculated on high-resolution confocal single optical planes of cerebellar cortex sections double-immunolabeled for CSPG4 and WGA-555 as the mean gray value (0–255 scale) of the green channel (ImageJ) using manual segmentation of whole plasmalemma and cytoplasm of single OPCs.

Oligodendrocyte analyses

Brains from postnatal day 20 pups were isolated, and sections were generated as aforementioned. For immunohistochemistry, slides were incubated in 5% NGS, 5% BSA, 0.1% Triton X-100 in PBS for 30 min, and then incubated with anti-glutathione-S-transferase-P antibody (1:2,000; MBL Life Science, Japan) in PBS with 5% NGS and 0.2% Triton X-100 overnight. Slides were washed and incubated in biotinylated anti-Rabbit secondary antibody (ABC Vectastain Kit; Vector Laboratories) (1% NGS and 0.2% Triton X-100 in PBS) containing ABC solutions (ABC Vectastain Kit; Vector Laboratories) for 2 h. After washing, slides were stained with 3,3'-diaminobenzidine (ImmPACT® DAB Substrate Kit; Vector Laboratories, Burlingame, CA) for 3 min, transferred to PBS, and mounted with DPX (Merck, NJ). Images were obtained and analyzed as aforementioned.

Lipidomic analyses

Ultracentrifugally isolated HDL fractions or cerebellar protein lysates were mixed with butanol/methanol and internal standards. HDL was isolated from 300 µl plasma using KBr density gradient ultracentrifugation as described (30) with some modifications (Thermo Fisher Technical note TNCFLIPOMICRO 0712, <https://tools.thermofisher.com/content/sfs/brochures/D21028~.pdf>). Following isolation, the HDL fraction was desalted following the manufacturer's protocol (Pierce 89849 Desalting Column; Thermo Fisher Scientific, Waltham, MA). Lipid extraction was performed as described (31). Quantification of lipid species was performed by LC-MS/MS using a 6460 QQQ (Agilent, Santa Clara, CA) mass spectrometer. A C18 Agilent Zorbax HHD, 50 Å~2.1 mm column was used for liquid chromatographic separation of

the lipids. Data were extracted and quantified using MassHunter Quant Software (Agilent).

Statistics

All experiments were quantified by experimenters blinded to the genotype. All data were tested for normality using the D'Agostino-Pearson omnibus normality test or the Shapiro-Wilk normality test for small sample sizes. Normal data were analyzed using parametric unpaired Student's *t*-test or two-way ANOVA. Non-normal data were analyzed using the nonparametric Mann-Whitney *U* test. For two-way ANOVA, multiple comparisons test was performed followed by Bonferroni correction. All statistical analyses were performed in GraphPad Prism 7 (GraphPad Software, Inc). *P* < 0.05 was considered significant. Results are shown as mean ± SEM.

RESULTS

Abca8b expression is highest in oligodendrocytes

ABCA8 was originally cloned as a gene with unknown function from human brain libraries (3). Two tandem gene orthologs exist for *ABCA8* in mice, *Abca8a*

and *Abca8b* (supplemental Fig. S1A). *Abca8b* shows 75% amino acid identity with human ABCA8, whereas *Abca8a* shows 69% identity (supplemental Table S2). To determine if *Abca8a* and *Abca8b* are expressed in the brain, we performed tissue expression analyses in adult *wild-type* mice and found little expression of *Abca8a* in the brain, whereas *Abca8b* was expressed at relatively higher levels (*Abca8a*: *n* = 4, *Abca8b*: *n* = 5; Fig. 1A). In agreement with our data, two studies utilizing in situ hybridization and quantitative PCR found robust expression of *Abca8b* in postnatal mouse brains, whereas the expression of *Abca8a* was almost indistinguishable (32, 33). Of the brain regions analyzed, *Abca8b* expression was highest in the cerebellum (Fig. 1B). In line with this, analyses of the human protein atlas showed that of the brain regions assessed, ABCA8 protein was most highly expressed in the cerebellum, where it was expressed in white matter processes and in the cytoplasm and plasma membranes of white matter cells (https://www.proteinatlas.org/ENSG00000141338-ABCA8/brain/cerebellum#ih_tissue). In silico analyses

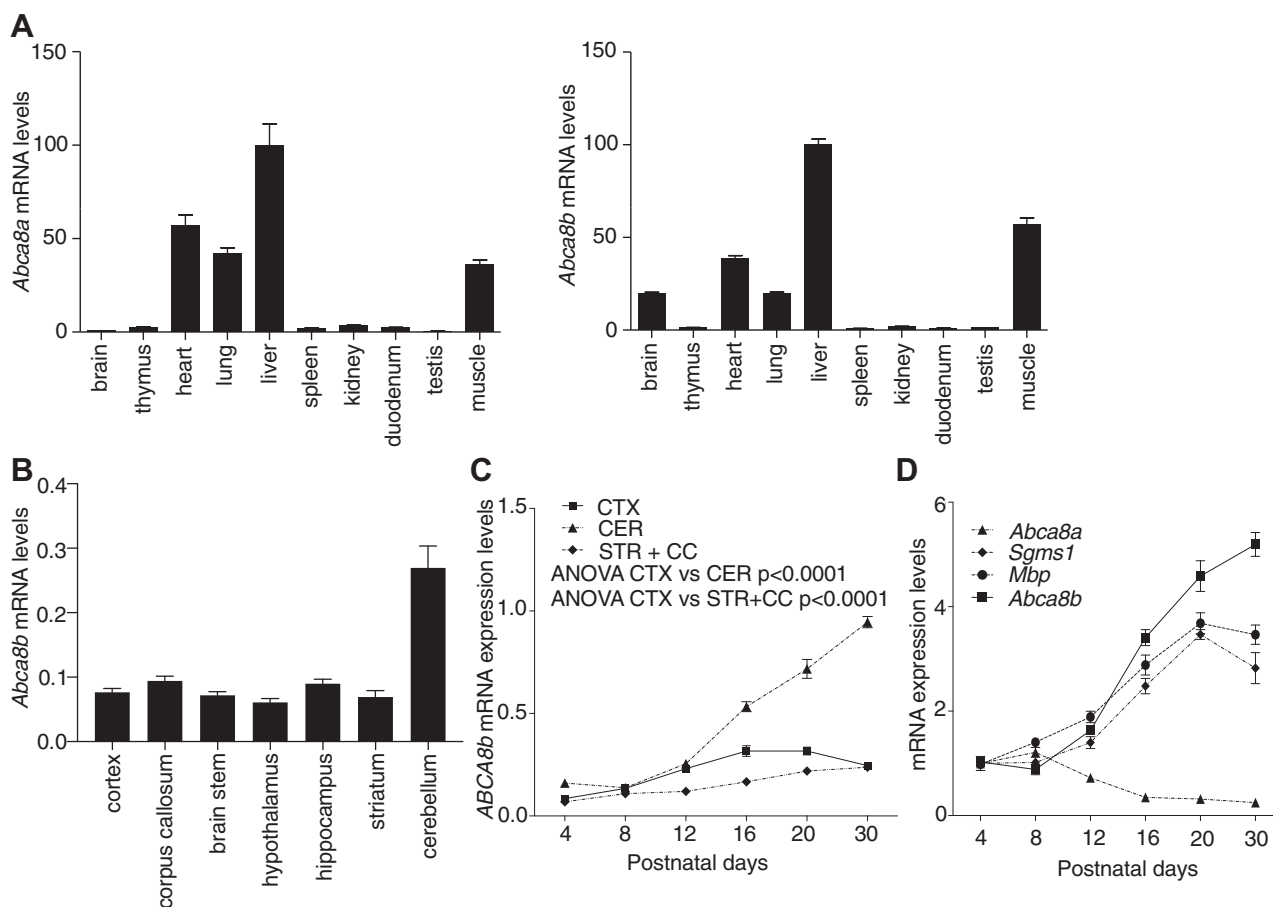


Fig. 1. *Abca8b* expression is highest in the cerebellum where it is substantially increased during the postnatal myelination phase in mice. A: RT-quantitative PCR analyses found that, compared with *Abca8a*, *Abca8b* expression is substantially increased in the brain of adult *wild-type* mice. Data were normalized to liver expression. *Abca8a*: *n* = 4; *Abca8b*: *n* = 5. B: Of the brain regions, *Abca8b* showed the highest expression in the cerebellum of *wild-type* mice. *n* = 5. C: During the postnatal phase of myelination, *Abca8b* expression is substantially increased in the cerebellum. *n* = 5 each. D: Expression of genes with established roles in myelination, *Sgms1* and *Mbp*, are increased in the cerebellum during the early postnatal phase of myelination, and coincide with an increase in *Abca8b* levels, whereas *Abca8a* levels are not increased in the early postnatal period. *n* = 5 each. Values are mean ± SEM. Data in (C) are analyzed by two-way ANOVA. CER, cerebellum; CTX, cortex; STR + CC, striatum + corpus callosum pooled samples.

of the “Barres atlas” showed that human *ABCA8* expression was highest in oligodendrocytes, whereas mouse *Abca8b* expression was highest in OPCs (34) (supplemental Fig. S1B). In this database, the expression of human genes was assessed in pooled brain samples from individuals 8–63 years old, whereas postnatal day 7 and 17 pups were used for the mouse expression atlas, perhaps explaining the oligodendrocytes versus OPC expression in humans versus mice. Since oligodendrocytes are the myelinating cells, these findings suggest that *ABCA8/Abca8b* might contribute to myelination, especially in the cerebellum.

Cerebellar *Abca8b* expression increases during the myelination phase and coincides with myelination gene expression in mice

Concurrent with oligodendrogenesis, the predominant portion of myelination in the mouse occurs in the early postnatal stage, between postnatal days 10 and 20, and the expression of the genes playing critical roles in myelination are highly increased during this early postnatal period (35). If *Abca8b* plays a role in myelination, its expression should also be increased during this early postnatal period. Compared with the cortex and pooled striatum/corpus callosum, *Abca8b* expression was significantly increased in the cerebellum of *wild-type* mice during the myelination phase between postnatal days 12 and 30 (*Abca8b* expression: cerebellum vs. cortex, $P < 0.0001$, ANOVA; cerebellum vs. striatum + corpus callosum, $P < 0.0001$, ANOVA; Fig. 1C). We next compared cerebellar *Abca8b* expression with the expression of the established myelination gene *Myelin basic protein (Mbp)* (36), and with *Sgms1*, a gene critical for the synthesis of sphingomyelin, an essential myelin lipid component (37). The postnatal increase in cerebellar *Abca8b* expression coincided with increased expression of both *Mbp* and *Sgms1* (Fig. 1D), further indicating a possible role for *Abca8b* in myelination. In contrast to *Abca8b* expression, which was increased by ~400% between postnatal days 4 and 20 in *wild-type* mice, no increase in *Abca8a* expression was found (Fig. 1D), suggesting that *Abca8b* might play a role in cerebellar myelination, whereas *Abca8a* is unlikely to do so.

Cerebellar hypoplasia with decreased cerebellar OPC and mature oligodendrocyte cell numbers in *Abca8b*^{-/-} mice

ABCA8/Abca8b is highly expressed in oligodendrocytes. To determine if *Abca8b* regulates OPC and/or mature oligodendrocyte (OL) function, thus leading to altered myelination, we first quantified cerebellar size and weight in our previously generated (12) *Abca8b*^{-/-} mice. Brain weights were decreased in 1-month-old *Abca8b*^{-/-} mice (*wt* 374.3 ± 4.7, n = 11; *Abca8b*^{-/-} 359.0 ± 4.7, n = 10; mg, $P = 0.03$) (Fig. 2A), arising from decreased cerebellar weight (*wt* 55.9 ± 1.5, n = 11;

Abca8b^{-/-} 48.9 ± 1.8, n = 10; mg, $P = 0.008$) (Fig. 2B), since forebrain weights were unchanged in *Abca8b*^{-/-} mice (*wt* 318.4 ± 4.0, n = 11; *Abca8b*^{-/-} 310.0 ± 4.4, n = 10; mg, $P = 0.2$) (Fig. 2C). As well, cerebellar area was decreased in *Abca8b*^{-/-} mice (*wt* 7.20 ± 0.12, n = 8; *Abca8b*^{-/-} 6.58 ± 0.15, n = 9; mm², $P = 0.006$) (Fig. 2D) suggesting an important role for *Abca8b* in brain development.

We found *Abca8b* highly expressed in OPCs and in the cerebellum in *wild-type* mice, and *ABCA8* was significantly upregulated during oligodendrogenesis (15, 24). Thus, we next assessed the number of OPCs in the developing *Abca8b*^{-/-} mouse cerebella, utilizing a specific marker of OPCs, platelet-derived growth factor receptor alpha (38). The deep cerebellar nuclei contain the main cerebellar outputs, and the developing white matter (dWM) is the myelin-enriched area of the cerebellum (39). Thus, OPC numbers were assessed in these areas. Postnatal days 4, 7, and 9 were chosen for analyses because the proliferation of OPCs is observed during this period in mice, with the highest cerebellar OPC numbers being observed on postnatal day 7 (40). The number of OPCs was reduced in the dWM of the cerebellum at postnatal days 7 and 9 in *Abca8b*^{-/-} mice (day 7: *wt* 341.7 ± 24.7, n = 4; *Abca8b*^{-/-} 248.9 ± 22.2, n = 4; cell number/mm², $P = 0.03$; day 9: *wt* 331.3 ± 22.9, n = 3; *Abca8b*^{-/-} 128.8 ± 14.5, n = 4; cell number/mm², $P = 0.0005$), whereas no changes were observed in OPC number at postnatal day 4 (*wt* 280.8 ± 15.7, n = 4; *Abca8b*^{-/-} 315.4 ± 28.1, n = 4; cell number/mm², $P = 0.3$) (Fig. 2E and supplemental Fig. S2). In addition, the numbers of OPCs in the deep cerebellar nuclei of the cerebellum was also reduced in *Abca8b*^{-/-} mice at postnatal days 7 and 9 (day 7: *wt* 567.4 ± 7.0, n = 4; *Abca8b*^{-/-} 463.5 ± 30.3, n = 4; cell number/mm², $P = 0.02$; day 9: *wt* 505.9 ± 46.6, n = 3; *Abca8b*^{-/-} 235.4 ± 23.9, n = 4; cell number/mm², $P = 0.003$), whereas no changes were observed at postnatal day 4 (*wt* 366.3 ± 11.9; *Abca8b*^{-/-} 387.6 ± 31.9; cell number/mm², n = 4 each, $P = 0.6$) (Fig. 2F and supplemental Fig. S2). Together, our data suggest that the absence of *Abca8b* in mice disrupted oligodendrogenesis in the cerebellum resulting in reduced OPC numbers.

With the ability to differentiate into myelin-producing OLs, OPC migration, proliferation, and differentiation are essential for generating cells of the oligodendrocyte lineage, and OPC number is positively linked with OL numbers (41). Since OPC numbers are decreased in *Abca8b*^{-/-} cerebella, we next assessed OL numbers by staining with glutathione-S-transferase- π , a marker for OLs (42). OLs were lower in the dWM in *Abca8b*^{-/-} mice at postnatal day 20, a time during which OLs and myelination gene expression are increased (*wt* 427.5 ± 58.4; *Abca8b*^{-/-} 182.0 ± 15.5; n = 5 each, cell number/mm², $P = 0.004$) (Fig. 2G). In addition, OLs in the deep cerebellar nuclei were also reduced (*wt* 761.3 ± 78.2; *Abca8b*^{-/-} 466.3 ± 26.6; n = 5 each, cell number/mm²; $P = 0.007$) (Fig. 2H). Together, decreases in OPCs

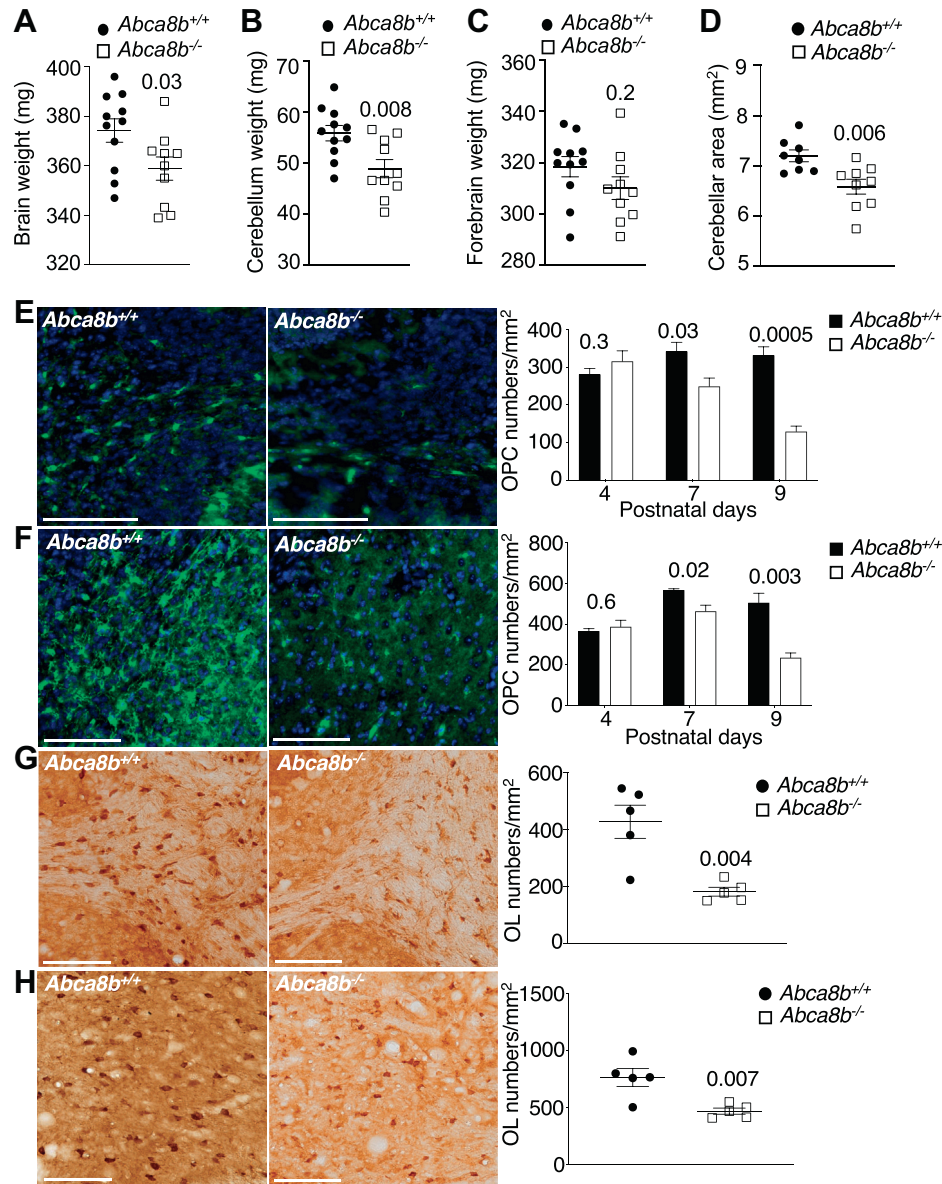


Fig. 2. Reduced cerebellar weight, area, OPC, and OL numbers in *Abca8b*^{-/-} mouse cerebella. **A:** Brain weights and **(B)** cerebellar weights are decreased in *Abca8b*^{-/-} mice. n = 11 each. **C:** Unchanged forebrain weights in *Abca8b*^{-/-} mice. n = 11 each. **D:** Decreased cerebellar area in *Abca8b*^{-/-} mice. n = 8–9. Decreased OPC numbers in the developing white matter **(E)** and deep cerebellar nuclei **(F)** of *Abca8b*^{-/-} mice. Images are from postnatal day 9. PDGFR α = green; DAPI = blue. Decreased OL numbers in the developing white matter **(G)** and deep cerebellar nuclei **(H)** of *Abca8b*^{-/-} mice. n = 5 each. Images are from postnatal day 20. Values represent mean \pm SEM. Data in A–D were normally distributed and analyzed using Student's *t*-tests. Data in E–H were not normally distributed and analyzed using Mann-Whitney *U* test. Scale bars in E–H represent 100 μ m. DAPI, 4',6-diamidino-2-phenylindole; PDGFR α , platelet-derived growth factor receptor alpha.

and OLs in the dWM and deep cerebellar nuclei suggest decreased myelination and disrupted cerebellar function in the absence of *Abca8b*.

ABCA8 interacts with the oligodendrocyte regulator CSPG4 in oligodendrocytes

To determine how ABCA8 might regulate oligodendrocyte numbers, we performed BioID assays, which screen for physiologically relevant protein interactions occurring in live cells (43). Since ABCA8 is highly expressed in oligodendrocytes and modulates OPC and

OL numbers, we used the MO3.13 human glial oligodendrocyte cell line. We identified two brain localized ABCA8-interacting proteins with links to myelination, CSPG4/neuron-glia antigen 2, and neuroblast differentiation-associated protein (AHNAK) (Fig. 3A). CSPG4 showed robust coimmunoprecipitation with ABCA8 (Fig. 3B), confirming the interaction between ABCA8 and CSPG4. Since the interaction of ABCA8 with CSPG4 was identified in all three rounds of BioID, and since CSPG4 promotes OPC proliferation, migration, and myelination (40), we performed further

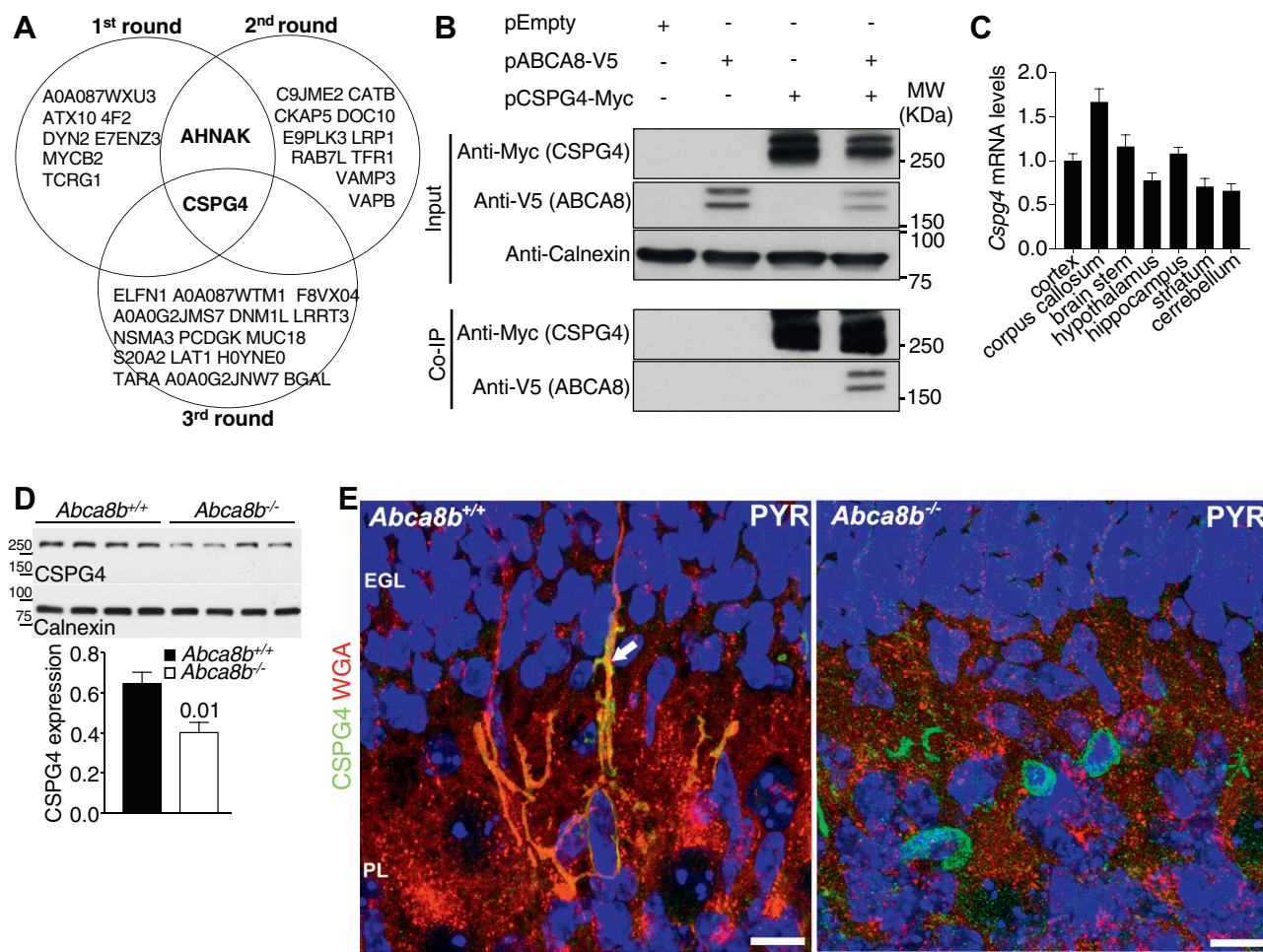


Fig. 3. ABCA8 interacts with CSPG4 whose levels and membrane localization are reduced in *Abca8b*^{-/-} cerebella. **A:** ABCA8 interacting proteins identified by BioID in human glial hybrid cell line. **B:** The interaction of ABCA8 with CSPG4 was confirmed using coimmunoprecipitation. **C:** *Cspg4* is expressed in the cerebellum, where its (D) protein levels ($n = 4$ each) are reduced postnatally in *Abca8b*^{-/-} mice. **E:** CSPG4 localizes with plasmalemmal WGA in cerebellar OPCs of the Purkinje layer (PL) in *Abca8b*^{+/+} (arrow) and not in *Abca8b*^{-/-} mice. Data were analyzed using Mann-Whitney *U* test. Scale bars in E represent 10 μ m. EGL, external granular layer; PYR, pyramis lobule; WGA, wheat germ agglutinin.

studies with this protein. AHNAK was only identified in two of the three rounds of BioID, is 700 kDa in size, and neither an antibody for immunoprecipitation nor a cDNA clone for AHNAK was available. Thus, this interaction was not confirmed.

Decreased CSPG4 expression and plasma membrane localization in *Abca8b*^{-/-} cerebella

In the CNS, CSPG4 is highly expressed in OPCs (44). As well, CSPG4 regulates OPC proliferation and migration, thus modulating myelination (40). To determine whether the absence of *Abca8b* affects the expression and/or localization of CSPG4, which might have contributed to the reduced oligodendrocyte population in *Abca8b*^{-/-} mice, we first confirmed that CSPG4 is expressed in the cerebellum in *wild-type* mice (Fig. 3C). In *Abca8b*^{-/-} mice, cerebellar CSPG4 protein levels were significantly decreased (*wt* 0.65 ± 0.05 ; *Abca8b*^{-/-} 0.41 ± 0.05 ; $n = 4$ each, relative expression, $P = 0.01$) (Fig. 3D).

Alteration in CSPG4 subcellular localization has been recently associated with reduced myelination in schizophrenia (45). To determine if the subcellular localization of CSPG4 was altered in the absence of *Abca8b*, we performed confocal microscopic analyses in mice at postnatal day 8. In the posterior cerebellar lobe of *wild-type* mice, CSPG4 showed high staining intensity and revealed long CSPG4⁺ processes originating from OPCs residing in the developing Purkinje layer and ascending to the developing external granular layer (Fig. 3E). In contrast, reduced CSPG4 staining was observed in the same regions of *Abca8b*^{-/-} mice, where CSPG4 staining did not show OPC processes ascending to the external granular layer (Fig. 3E). An in-depth analysis of subcellular CSPG4 immunoreactivity in *wild-type* mice found CSPG4 on the plasma membrane of OPCs, where it extensively colocalized with the membrane marker WGA (supplemental Fig. S3A, B). In *Abca8b*^{-/-} mice, CSPG4 appeared preferentially located intracellularly and scarcely colocalized with WGA at

the plasma membrane (supplemental Fig. S3A, B). Quantitative analyses revealed significantly increased plasma membrane CSPG4/WGA colocalization by Pearson's coefficient, Mander's colocalization coefficients (M1 and M2), threshold overlap score linear metric, and signal intensity correlation in *wild-type* mice (supplemental Fig. S3C–F). In addition, the mean fluorescence intensity (expressed as mean gray value) of CSPG4 located in cytoplasm of OPCs was significantly increased in *Abca8b*^{-/-} mice (*wt* 20865.8 ± 5024.3, n = 6; *Abca8b*^{-/-} 131490.1 ± 23991.5, n = 7; relative expression, *P* = 0.002) (supplemental Fig. S3G). Conversely, CSPG4 embedded in OPC plasma membrane appeared significantly decreased in *Abca8b*^{-/-} mice (*wt* 156925.2 ± 12702.1, n = 6; *Abca8b*^{-/-} 75827.6 ± 16484.3, n = 7; relative expression, *P* = 0.003) (supplemental Fig. S3H). These quantifications confirmed that CSPG4 levels and its plasma membrane localization are reduced in the absence of *Abca8b* in cerebellar OPCs.

Altered cerebellar distribution and morphology of CSPG4-positive OPCs in *Abca8b*^{-/-} mice

In addition to the reduced cerebellar OPC and OL numbers in the absence of *Abca8b*, to investigate whether the decreased expression and subcellular localization of CSPG4 could affect the cerebellar distribution of CSPG4⁺ OPCs or their morphology, we performed immunofluorescence-based morphological and morphometrical confocal analyses of the mice at postnatal day 8, a time when the majority of OPCs have migrated from subependymal layers of the fourth ventricle to developing cerebellar folia along a ventrodorsal and caudorostral route (46). The distribution of CSPG4⁺ OPCs appeared ubiquitous in the different cerebellar folia in the *wild-type* mice, with the highest density observed in the central dWM tracts, developing Purkinje layer, and developing internal granule layers, with lower density in the developing external granular layer (Fig. 4A, B). In contrast, CSPG4⁺ OPCs were reduced in number according to the distance of the folia from the fourth ventricle and superior medullary velum in *Abca8b*^{-/-} cerebella (Fig. 4A, B). The most dorsal folia such as pyramis (VIII), paramedian (VIII), and ansiform lobules (VI and VII) contained few and weakly CSPG4-stained OPCs in *Abca8b*^{-/-} mice (Fig. 4A, B), whereas the ventral folia appeared similar to the *wild-type* mice (Fig. 4B).

Considering that the altered subcellular localization of CSPG4 could modify the cell shape and process extension, morphological characteristics of OPCs were in addition quantified and described by a series of morphometric parameters. The calculated number of CSPG4⁺ OPC processes (end points) and their length were reduced in *Abca8b*^{-/-} mice (number of end points per cell: *wt* 1301.4 ± 7.6; *Abca8b*^{-/-}: 465.0 ± 63.9, n = 5 each; *P* < 0.0001; sum of branch length in micrometer: *wt* 1037.9 ± 75.1; *Abca8b*^{-/-}: 466.2 ± 24.3, n = 5 each; *P* < 0.0001) (Fig. 4C, D). Conversely, morphological complexity (fractal dimension) and shape heterogeneity (lacunarity)

did not differ between the two genotypes (Fig. 4C, D). Together, these data suggest that the absence of *Abca8b* results in CSPG4 dysfunction, leading to reduced OPC and OL numbers, and resulting in altered cerebellar distribution and morphology in the remaining cerebellar OPCs.

Myelination is decreased in *Abca8b*^{-/-} mice

To directly assess whether cerebellar myelination levels are reduced in the *Abca8b*^{-/-} mice, we performed Black-Gold II staining for myelin in mice at postnatal day 20. Staining intensity was decreased in the deep cerebellar nuclei (*wt* 0.61 ± 0.02; *Abca8b*^{-/-}: 0.46 ± 0.01, percent of Black-Gold positive area, n = 10 each, *P* < 0.0001; Fig. 5A) and in the dWM region (*wt* 0.90 ± 0.01; *Abca8b*^{-/-}: 0.78 ± 0.01, percent of Black-Gold positive area, n = 10 each, *P* < 0.0001; Fig. 5B) of *Abca8b*^{-/-} mice.

We also assessed the expression of genes playing a role in myelination, 2',3'-cyclic nucleotide 3' phosphodiesterase (*Cnp*), proteolipid protein 1 (*Plp1*), and myelin oligodendrocyte glycoprotein (*Mog*) (47), in *Abca8b*^{-/-} cerebella, during the early postnatal myelination phase. The expression of *Cnp* (day 16: *wt* 21.5 ± 0.5; *Abca8b*^{-/-}: 15.4 ± 1.3, relative expression, n = 4 each, *P* = 0.03; day 20: *wt* 23.7 ± 0.8; *Abca8b*^{-/-}: 18.1 ± 0.6, relative expression, n = 4 each, *P* = 0.01), *Plp1* (day 16: *wt* 107.6 ± 6.3; *Abca8b*^{-/-}: 84.8 ± 6.6, relative expression, n = 4 each, *P* = 0.047; day 20: *wt* 137.5 ± 3.2; *Abca8b*^{-/-}: 97.1 ± 2.3, relative expression, n = 4 each, *P* = 0.0001), and *Mog* (day 16: *wt* 619.4 ± 49.2; *Abca8b*^{-/-}: 361.5 ± 36.4, relative expression, n = 4 each, *P* = 0.006; day 20: *wt* 708.1 ± 47.9; *Abca8b*^{-/-}: 387.5 ± 36.2, relative expression, n = 4 each, *P* = 0.002) were decreased at the early postnatal stage in *Abca8b*^{-/-} mice (Fig. 5C–E). Together, these data show cerebellar hypomyelination in the *Abca8b*^{-/-} mice.

Disordered myelin ultrastructure in *Abca8b*^{-/-} mice

To examine whether the lack of *Abca8b* altered myelin sheath ultrastructure, we performed electron microscopic analyses of the cerebella of 1-month-old *Abca8b*^{-/-} mice (Fig. 6A). Markedly greater numbers of unmyelinated axons were observed in *Abca8b*^{-/-} mice (*wt* 3.2 ± 0.3; *Abca8b*^{-/-}: 11.8 ± 1.6, number of unmyelinated axons/100 μm², n = 5 each, *P* = 0.0008) (Fig. 6B). We next assessed the g-ratio, a measure of myelin sheath thickness, in the mice (48) and found it to be higher in *Abca8b*^{-/-} mice (*wt* 0.680 ± 0.003, n = 798; *Abca8b*^{-/-}: 0.738 ± 0.003, n = 833, *P* = 0.0001; Fig. 6C), indicating reduced myelin sheath thickness. Direct quantification of myelin sheath thickness showed it to be decreased in *Abca8b*^{-/-} mice (*wt* 0.391 ± 0.006, n = 798; *Abca8b*^{-/-}: 0.213 ± 0.004, n = 833, micrometer, *P* = 0.0001; Fig. 6D). Axon diameter was also decreased in *Abca8b*^{-/-} mice (*wt* 0.90 ± 0.02, n = 798; *Abca8b*^{-/-}: 0.66 ± 0.01, n = 833, micrometer, *P* = 0.0001) (Fig. 6E). Plotting g-ratios against axonal diameters demonstrated that the g-ratios of larger caliber axons were reduced in *wild-type* mice, compared with *Abca8b*^{-/-} littermates, further

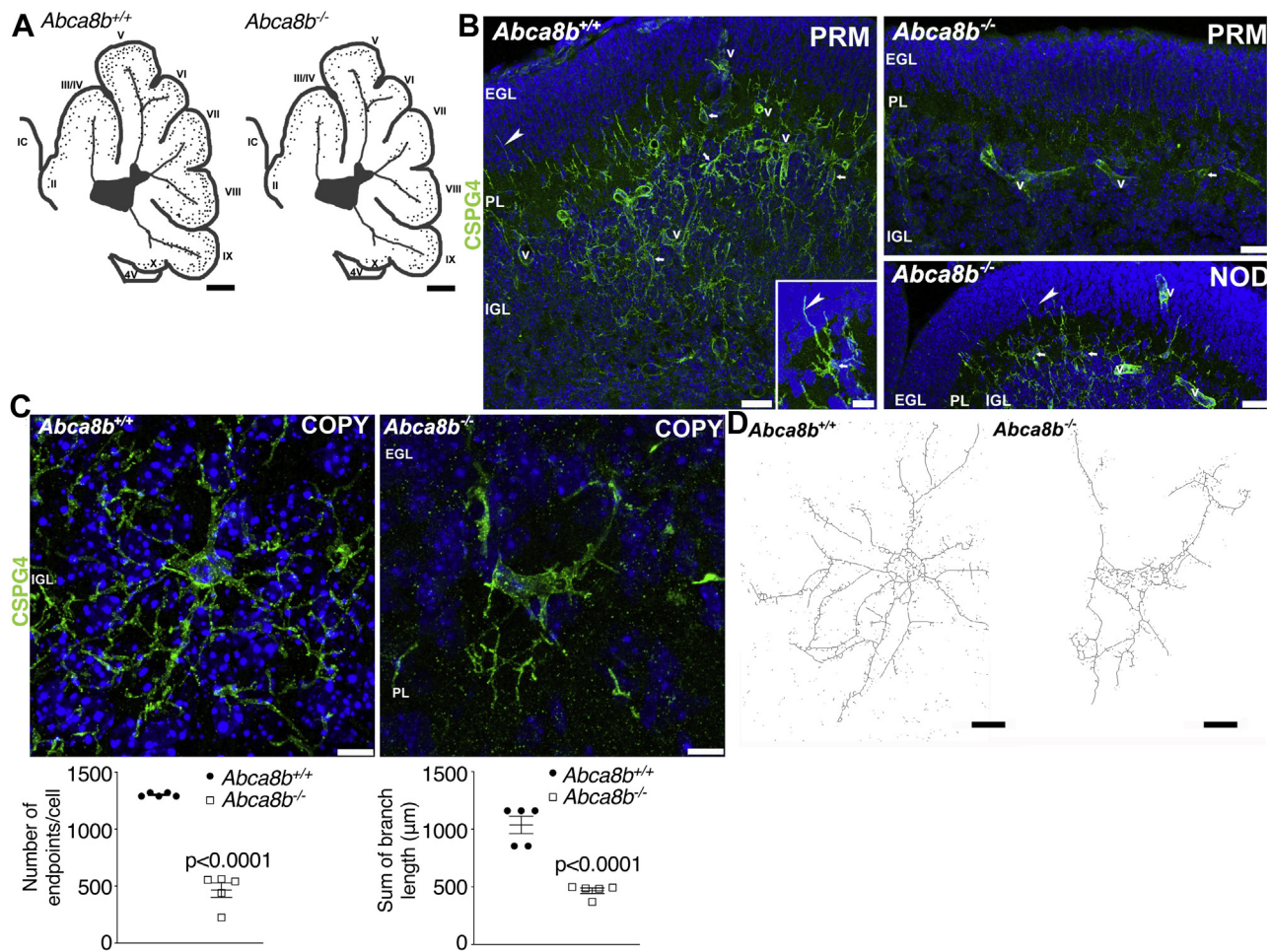


Fig. 4. Reduced CSPG4⁺ oligodendrocyte numbers and altered OPC morphology in *Abca8b*^{-/-} cerebella. A: Schematic showing reduced numbers of CSPG4⁺ OPCs in the posterior cerebellar lobules of *Abca8b*^{-/-} mice. B: Reduced CSPG4 expression and CSPG4⁺ OPCs (arrows) in the paramedian lobule (PRM) of *Abca8b*^{-/-} cerebella, whereas longer OPC processes (arrowheads and inset) appear to ascend from the Purkinje layer (PL) to the external granular layer (EGL) in *Abca8b*^{+/+} mice. These differences are absent in the anterior and flocculonodular cerebellar lobes (NOD). Microvascular pericytes (v) also express CSPG4 and appear unaffected in *Abca8b*^{-/-} mice. C: Reduced CSPG4⁺ OPC end points and process lengths in *Abca8b*^{-/-} mice, which is better evidenced by cell skeleton analyses and quantified in (D). Scale bars in A represent 1 mm, (B): 25 μm, (B inset): 10 μm; and (C, D): 7.5 μm. COPY, copula pyramidis lobe; IGL, internal granular layer.

indicating reduced myelin thickness in *Abca8b*^{-/-} mice (difference in slopes, $P = ns$; difference between constants $P < 0.0001$) (Fig. 6F). The periodicity of the myelin sheath was also decreased in *Abca8b*^{-/-} mice (wt 5.50 ± 0.21 , $n = 5$; *Abca8b*^{-/-}: 4.83 ± 0.20 , $n = 5$, nanometer, $P = 0.049$) (Fig. 6G), indicating increased compaction of the myelin sheath. Together, these data show that *Abca8b* plays an important role in modulating cerebellar myelin sheath ultrastructure.

Slower cerebellar signal conduction velocity in *Abca8b*^{-/-} mice

To determine if the disturbed myelination resulted in functional defects in the *Abca8b*^{-/-} mice, we measured the latency of compound action potentials, to quantify the conduction velocity of electric signals through axonal fibers in *Abca8b*^{-/-} cerebella at 1 month of age. Latencies were measured at two different sites, 0.5 and 1.0 mm away from the site of

the stimulation electrode. The latencies of signal propagation at 1 mm were significantly increased in *Abca8b*^{-/-} mice (*Abca8b*^{+/+}: 5.67 ± 0.19 , $n = 5$ mice, $n = 14$ slices; *Abca8b*^{-/-}: 6.20 ± 0.14 , $n = 5$ mice, $n = 13$ slices, milliseconds, $P = 0.036$), whereas the increased latency in signal propagation at 0.5 mm trended toward significance (*Abca8b*^{+/+}: 3.63 ± 0.17 , $n = 5$, $n = 14$; *Abca8b*^{-/-}: 4.07 ± 0.16 , $n = 5$, $n = 13$, milliseconds, $P = 0.07$; Fig. 7A–C). These results suggest that the decreased cerebellar myelination and the disordered myelin sheath ultrastructure led to decreased conduction velocity in cerebellar fibers, and consequently, disturbed cerebellar function in *Abca8b*^{-/-} mice.

Disturbed locomotion in *Abca8b*^{-/-} mice

The cerebellum is critical in regulating movement and locomotor activity, and controls posture, tone, flexion, and extension of limbs (49). To determine if

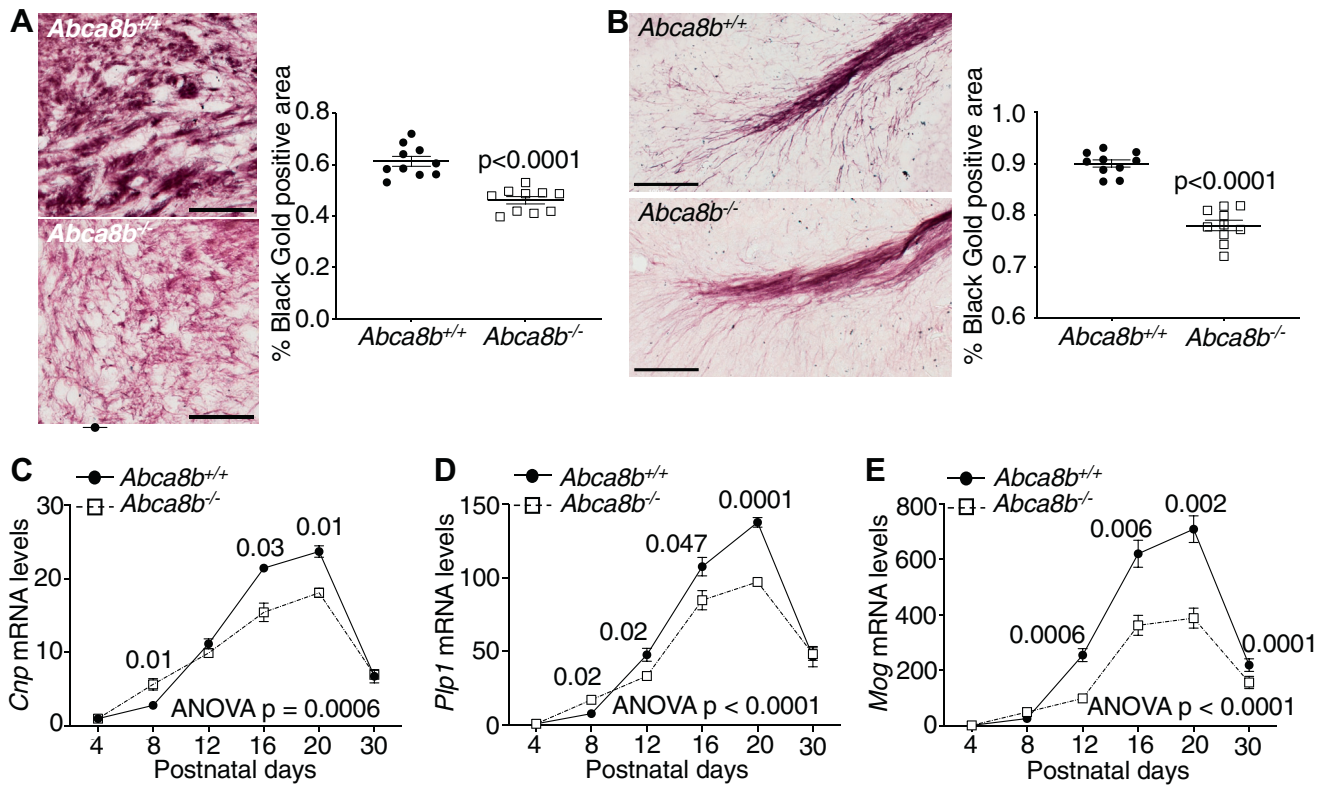


Fig. 5. Myelination levels and myelination gene expression are decreased in the cerebella of *Abca8b*^{-/-} mice. Myelination levels are decreased in the deep cerebellar nuclei (A) and in the developing white matter (B) of the cerebellum in the *Abca8b*^{-/-} mice. $n = 10$ each. Expression levels of the myelination genes *Cnp* (C), *Plp1* (D), and *Mog* (E) are decreased in the cerebella of *Abca8b*^{-/-} mice. $n = 5$ each. Values are mean \pm SEM. Data in (A, B) were normally distributed and analyzed using Student's *t*-tests. Data in (C–E) are analyzed by one-way ANOVA, and individual data points were normally distributed and analyzed using Student's *t*-tests. The scale bar in A and B represents 100 μ m.

the reduced myelination and slower cerebellar conduction velocity observed in *Abca8b*^{-/-} mice resulted in altered locomotion, we performed gait testing of the *Abca8b*^{-/-} mice at 6 weeks of age. Significantly decreased stride width (*wt.* 2.38 ± 0.06 ; *Abca8b*^{-/-}: 2.07 ± 0.04 , centimeters, $n = 5$ each, $P = 0.003$) (Fig. 7D) and toe spread width (*wt.* 8.70 ± 0.15 ; *Abca8b*^{-/-}: 7.90 ± 0.19 , millimeter, $n = 5$ each, $P = 0.03$) (Fig. 7E) were observed in the *Abca8b*^{-/-} mice. No changes in stride length were observed (*wt.* 6.93 ± 0.25 ; *Abca8b*^{-/-}: 7.12 ± 0.11 , centimeter, $n = 5$ each, $P = 0.5$) (data not shown). No changes in femur lengths were observed in the mice, suggesting that the altered gait did not arise from smaller limb size (Fig. 7F). These data suggest that the reduced cerebellar myelination levels and slower cerebellar conduction velocity in the *Abca8b*^{-/-} mice resulted in dysfunctional cerebellar control of locomotion.

DISCUSSION

We establish here a causal and protective role for *Abca8b*, the brain-predominant mouse ortholog of human ABCA8, in cerebellar myelination. The absence of *Abca8b* decreased myelination in the cerebellum, leading to impaired cerebellar conduction velocity and impaired locomotor activity. Decreased

cerebellar OPC and OL cell numbers contributed to the decreased myelination. CSPG4 is expressed in OPCs and is essential for OPC proliferation, migration, differentiation into myelinating oligodendrocytes, and myelination (40). We found that ABCA8 interacts with CSPG4, and decreased levels of CSPG4 at its site of function at the plasma membrane likely contributed to the phenotypes in the *Abca8b*^{-/-} mice. In line with a role for ABCA8 in myelination, ABCA8 expression was increased in human neurological conditions with white matter dysfunction (16–19), perhaps as compensation for impaired myelination, and the ABCA8 gene locus was associated with multiple sclerosis, a disease characterized by white matter dysfunction (15). Together, our data suggest that increasing ABCA8 levels or activity may prove useful in treating neurological diseases with white matter dysfunction.

Deficits in myelination and white matter integrity are well-defined characteristics of schizophrenia (50). A genetic study of familial schizophrenia identified reduced brain white matter integrity in carriers of mutations in *CSPG4*, and the plasma membrane localization of CSPG4 was found to be essential for its regulation of myelination (45). In line with this, CSPG4 requires plasma membrane lipid raft localization for its

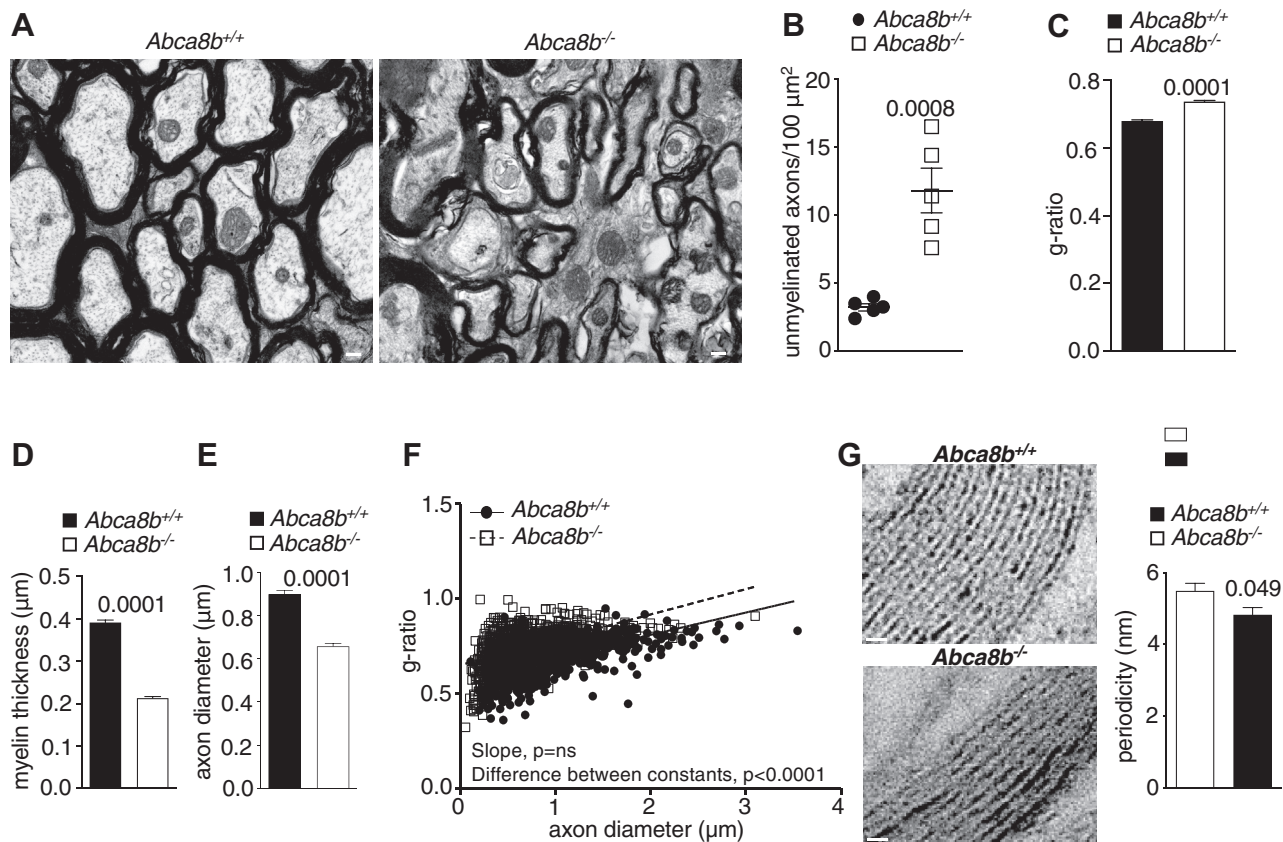


Fig. 6. Disordered cerebellar myelin structure in *Abca8b*^{-/-} mice. A: Electron microscopy images of the cerebella of *Abca8b*^{+/+} and *Abca8b*^{-/-} mice. Increased number of unmyelinated axons (B), increased g-ratio (C), decreased myelin sheath thickness (D), and decreased axon diameter (E) in the cerebella of *Abca8b*^{-/-} mice. F: Plot of g-ratio versus axon diameter indicating reduced myelin thickness. G: Decreased myelin sheath periodicity in *Abca8b*^{-/-} mice. Values are mean \pm SEM, n = 5 mice per group. Data in (B–E) and (G) were normally distributed and analyzed using Student's *t*-tests. Data in (F) were analyzed using ANCOVA. Scale bars in (A) represent 0.2 μ m and (G) represent 20 nm.

function (51). We found that CSPG4 expression and its plasma membrane localization in OPCs were decreased in *Abca8b*^{-/-} cerebella. ABCA8 facilitates lipid efflux to extracellular HDL acceptor particles, suggesting that ABCA8 likely facilitates the transport of these lipids to the plasma membrane and/or from the plasma membrane to the HDL particles. Thus, ABCA8 may facilitate the formation of plasma membrane domains with specific lipid composition that may be essential for the proper localization and thus function of CSPG4. ABCA8 may also ensure the proper membrane localization of CSPG4 through its interaction with CSPG4, thus retaining it at plasma membrane domains.

Further evidence that CSPG4 dysfunction in the absence of ABCA8 may be a major contributor to the *Abca8b*^{-/-} phenotype is that *Cspg4*^{-/-} mice show overlapping phenotypes with the *Abca8b*^{-/-} mice. Although *Cspg4* is distributed widely in the brain (Fig. 3C), *Abca8b* shows an almost three times increased expression in the cerebellum compared with other brain regions (Fig. 1B). Interestingly, as in the absence of *Abca8b*, the absence of CSPG4 predominantly affected myelination in the cerebellum despite being widely expressed. Both mice show reduced numbers of OPCs in developing

cerebellar white matter in the early postnatal period, leading to reductions in both OLs and cerebellar myelination (40). As well, both mouse models show disrupted cerebellar OPC maturation and altered OPC morphology (40). These findings suggest that the impact of ABCA8 on myelination may indeed be modulated via CSPG4.

Besides its CSPG4-mediated role in myelination, if ABCA8 modulates myelination via additional mechanisms is uncertain. We previously found that ABCA8 facilitates the transport of cellular cholesterol to extracellular apolipoprotein A-I acceptor particles, thus increasing HDL cholesterol levels (12). In addition to reduced cholesterol levels, lipidomic analyses of HDL particles from heterozygous human carriers of loss-of-function mutations in ABCA8 also identified specific and significant decreases in plasmalogen phosphatidylethanolamine (PEtn) levels (supplemental Fig. S4A–C), suggesting that ABCA8 may also facilitate the transport of PEtn. Interestingly, phospholipids are the most abundant lipids by weight in myelin, and the most abundant phospholipid in myelin is PEtn (52). Indeed, brain plasmalogen levels increase substantially during the early postnatal developmental phase of

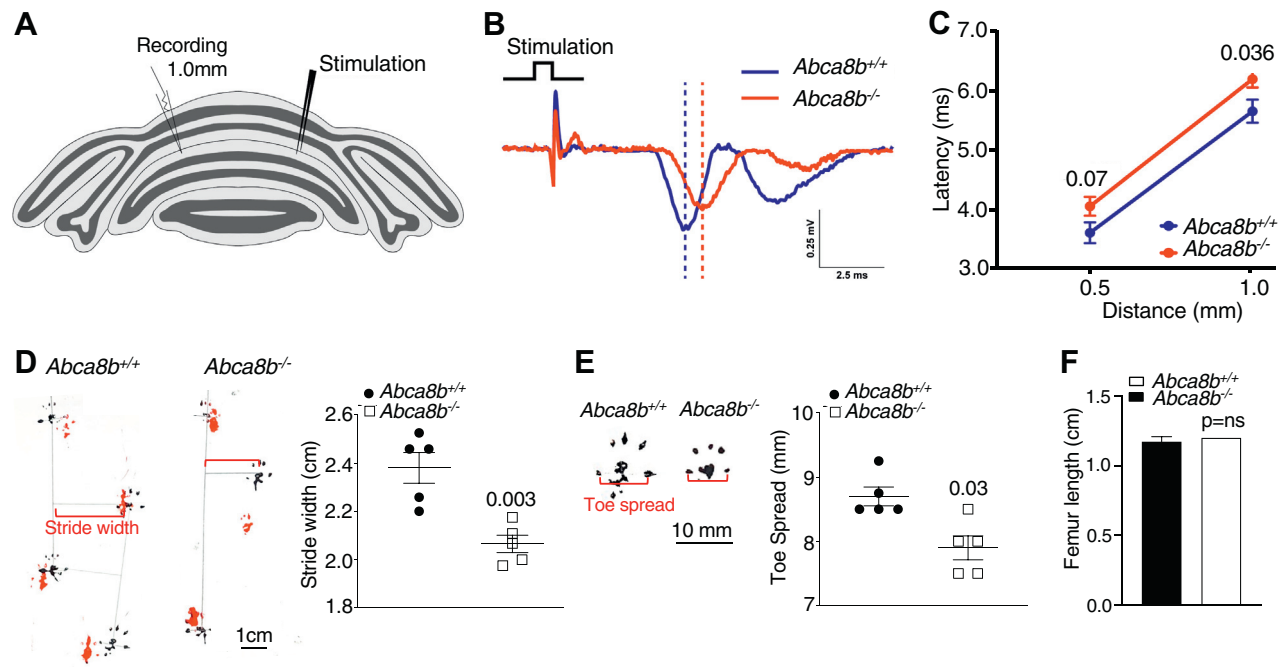


Fig. 7. Delayed cerebellar compound action potentials and altered gait in the *Abca8b*^{-/-} mice. A: The latencies of compound action potentials were measured in cerebellar parallel fibers at 0.5 and 1.0 mm of propagation distances in each group (*Abca8b*^{+/+}, n = 5 mice, n = 14 slices; *Abca8b*^{-/-}, n = 5 mice, n = 13 slices). B: The representative traces of compound action potential at 1.0 mm propagation are shown. C: The latencies at 1.0 mm propagation were significantly delayed in *Abca8b*^{-/-} mice, whereas the difference at 0.5 mm propagation showed a trend to delay, indicating slower neuroconduction in the cerebella of *Abca8b*^{-/-} mice. During gait testing, the *Abca8b*^{-/-} mice showed significantly decreased stride width (D) and significantly decreased toe spread (E), n = 5 each. F: Femur length was not altered in the *Abca8b*^{-/-} mice, n = 4 each. Values represent mean ± SEM. Data were not normally distributed and analyzed using the Mann-Whitney *U* test.

myelination, with the cerebellum containing high levels of plasmalogens (53). As well, prevention of plasmalogen synthesis via the reduction or abrogation of glyceronephosphate O-acyltransferase resulted in delayed or decreased myelination, abnormal white matter, and cerebellar atrophy in both humans and mice (54, 55). These findings together suggest that ABCA8 may modulate myelination by directly regulating myelin lipid content. However, lipidomic analyses of the cerebella of *Abca8b*^{-/-} mice showed no significant differences in the levels of PETn or other lipids (supplemental Fig. S4D). However, lipidomic analyses of purified myelin from whole brain showed decreased total PETn and sphingomyelin. As well, individual species of PETns, phosphatidylserines, and phosphatidylcholines were decreased (supplemental Table S3). These findings were mirrored in myelin isolated from the cerebella, which showed reduced total PETn and phosphatidylcholine levels, and individual species of PETns, phosphatidylserines, and phosphatidylcholines were decreased in the *Abca8b*^{-/-} mice (supplemental Table S4). Further studies are necessary to determine if ABCA8-mediated changes in OPC/OL membrane domain lipid levels are affected in the absence of ABCA8. However, this mechanism is unlikely to be a major contributor to the myelin defects observed in the absence of ABCA8, since OPC and mature myelinating

oligodendrocyte numbers are substantially decreased in the *Abca8b*^{-/-} mice, and it is unlikely that reduced myelin lipid content leads to decreased OPCs and oligodendrocytes.

In addition to CSPG4, ABCA8 also interacted with several other proteins, including AHNAK in our BioID assays. AHNAK plays a role in the morphology and motility of Schwann cells, which are the myelinating cells in the PNS (56), whereas oligodendrocytes are the myelinating cells in the CNS. AHNAK is also present in the CNS, and its levels are altered in AD hippocampus and cerebellum (57). Thus, CSPG4 dysfunction in the absence of ABCA8 may not be the sole contributor to the myelination phenotypes in the *Abca8b*^{-/-} mice. If ABCA8 also affects myelination in the PNS and/or if disturbed AHNAK in the absence of ABCA8 contributes to the altered cerebellar myelination remains to be studied.


We found previously that ABCA8 colocalizes with ABCA1 at the plasma membrane, coimmunoprecipitates with ABCA1, and ABCA8 potentiates the cholesterol efflux mediated by ABCA1 (12), suggesting that ABCA1 and A8 may work in concert to regulate lipid transport. As in the *Abca8b*^{-/-} mice, brain-specific *Abca1*^{-/-} mice exhibit reduced myelinated axons and decreased thickness of their myelin sheaths (6). Together, these findings suggest that ABCA1 may play

a role in the regulation of myelination by ABCA8, and further studies are needed to assess this possibility.

If reduced or absent ABCA8 in humans will lead to white matter dysfunction remains unclear. Interestingly, in a genome-wide association study, *rs16973424*, a missense variant in *ABCA8*, is associated with decreased age of onset of AD, which is increasingly recognized as a neurodegenerative disease with gray and white matter dysfunctions. In addition, another variant, *rs144216026*, is associated with increased late-onset AD (58, 59). As well, although the ABCA8-interacting protein CSPG4 is enriched in oligodendrocytes, if reduced CSPG4 levels affect white matter in humans remained unclear. However, a more recent study found that individuals with a rare missense mutation in *CSPG4* displayed reduced brain white matter integrity, when compared with unaffected sibling and matched general population controls (45). Together, these data suggest that our findings in mice that *Abca8b* regulates myelination via its interaction with CSPG4 may extend to humans.

Overall, we find that the absence of *Abca8b* decreases cerebellar myelination, in part through a CSPG4-mediated mechanism. Our studies raise the possibility that increasing ABCA8 may be beneficial in diseases with myelin dysfunction.

Data availability

This study includes no data deposited in external repositories. All data are available from the corresponding author upon reasonable request. 

Supplemental data

This article contains [supplemental data](#).

Acknowledgments

Microscopy data and images for Figs. 2 and 5 were acquired and analyzed in the SBIC-Nikon Imaging Centre at Biopolis, A*STAR, Singapore.

Author contributions

R. R. S. conceptualization; Y. L., D. C., L. T.-M., J. O., F. G., D. V., D.-G. J., H.-G. B., S. P. N., and F. T. formal analyses; Y. L., D. C., L. T.-M., J. O., F. G., D. V., D.-G. J., H.-G. B., S. P. N., and F. T. investigation; S. J., J. G., K. A. R., D.-G. J., F. T., D. V., and R. R. S. resources; R. R. S. writing—original draft; D. C., Y. L., L. T.-M., K. A. R., S. J., J. G., F. G., and D. V. writing—review and editing; R. R. S. supervision; R. R. S. project administration; R. R. S., and K. A. R. funding acquisition.

Author ORCID

Yiran Liu  <https://orcid.org/0000-0002-9935-7768>

Laia Trigueros-Motos  <https://orcid.org/0000-0002-4566-4738>

Han-Gyu Bae  <https://orcid.org/0000-0001-7542-552X>

Sangyong Jung  <https://orcid.org/0000-0003-3017-1145>

Roshni R. Singaraja  <https://orcid.org/0000-0002-3418-3867>

Funding and additional information

The studies were funded by the Agency for Science, Technology and Research, Singapore (to R. R. S.), The National University of Singapore (to R. R. S.), and an Australian National Health and Medical Research Council/Singaporean Biomedical Research Council joint program grant (to K. A. R./R. R. S.).

Conflict of interest

The authors declare that they have no conflicts of interest with the contents of this article.

Abbreviations

AD, Alzheimer's disease; apoE, apolipoprotein E; cDNA, complementary DNA; *Cnp*, 2',3'-cyclic nucleotide 3' phosphodiesterase; *CSPG4*, chondroitin sulfate proteoglycan 4; dWM, developing white matter; EGL, external granular layer; *Mbp*, myelin basic protein; *Mog*, myelin oligodendrocyte glycoprotein; NGS, normal goat serum; OPC, oligodendrocyte precursor cell; PETn, phosphatidylethanolamine; PFA, paraformaldehyde; *Ptp1*, proteolipid protein 1; PNS, peripheral nervous system; SBIC, Singapore Bioimaging Consortium; *SGMS1*, sphingomyelin synthase 1; WGA, wheat germ wheat germ agglutinin.

Manuscript received July 26, 2021, and in revised form October 31, 2021. Published, JLR Papers in Press, November 6, 2021, <https://doi.org/10.1016/j.jlr.2021.100147>

REFERENCES

- Vasiliou, V., Vasiliou, K., and Nebert, D. W. (2009) Human ATP-binding cassette (ABC) transporter family. *Hum. Genomics* **3**, 281–290
- Piehlner, A. P., Ozcürümez, M., and Kaminski, W. E. (2012) A subclass ATP-binding cassette proteins in brain lipid homeostasis and neurodegeneration. *Front. Psychiatry* **3**, 17
- Kim, W. S., Weickert, C. S., and Garner, B. (2008) Role of ATP-binding cassette transporters in brain lipid transport and neurological disease. *J. Neurochem* **104**, 1145–1166
- Hirsch-Reinshagen, V., Zhou, S., Burgess, B. L., Bernier, L., McIsaac, S. A., Chan, J. Y., Tansley, G. H., Cohn, J. S., Hayden, M. R., and Wellington, C. L. (2004) Deficiency of ABCA1 impairs apolipoprotein E metabolism in brain. *J. Biol. Chem.* **279**, 41197–41207
- Hirsch-Reinshagen, V., Burgess, B. L., and Wellington, C. L. (2009) Why lipids are important for Alzheimer disease? *Mol. Cell. Biochem.* **326**, 121–129
- Li, L., Li, R., Zacharek, A., Wang, F., Landschoot-Ward, J., Chopp, M., Chen, J., and Cui, X. (2020) ABCA1/ApoE/HDL signaling pathway facilitates myelination and oligodendrogenesis after stroke. *Int. J. Mol. Sci.* **21**, 4369
- Mack, J. T., Beljanski, V., Soulika, A. M., Townsend, D. M., Brown, C. B., Davis, W., and Tew, K. D. (2007) “Skittish” *Abca2* knockout mice display tremor, hyperactivity, and abnormal myelin ultrastructure in the central nervous system. *Mol. Cell. Biol.* **27**, 44–53
- Sakai, H., Tanaka, Y., Tanaka, M., Ban, N., Yamada, K., Matsuura, Y., Watanabe, D., Sasaki, M., Kita, T., and Inagaki, N. (2007) ABCA2 deficiency results in abnormal sphingolipid metabolism in mouse brain. *J. Biol. Chem.* **282**, 19692–19699
- Chan, S. L., Kim, W. S., Kwok, J. B., Hill, A. F., Cappai, R., Rye, K. A., and Garner, B. (2008) ATP-binding cassette transporter A7 regulates processing of amyloid precursor protein in vitro. *J. Neurochem.* **106**, 793–804
- De Roeck, A., Van Broeckhoven, C., and Sleegers, K. (2019) The role of ABCA7 in Alzheimer's disease: evidence from genomics, transcriptomics and methylomics. *Acta Neuropathol.* **138**, 201–220

11. Sakae, N., Liu, C. C., Shinohara, M., Frisch-Daiello, J., Ma, L., Yamazaki, Y., Tachibana, M., Younkin, L., Kurti, A., Carrasquillo, M. M., Zou, F., Sevlever, D., Biscoglio, G., Gan, M., Fol, R., *et al.* (2016) ABCA7 deficiency accelerates amyloid- β generation and Alzheimer's neuronal pathology. *J. Neurosci.* **36**, 3848–3859
12. Trigueros-Motos, L., van Capelleveen, J. C., Torta, F., Castaño, D., Zhang, L. H., Chai, E. C., Kang, M., Dimova, L. G., Schimmel, A., Tietjen, I., Radomski, C., Tan, L. J., Thiam, C. H., Narayanaswamy, P., Wu, D. H., *et al.* (2017) ABCA8 regulates cholesterol efflux and high-density lipoprotein cholesterol levels. *Arterioscler. Thromb. Vasc. Biol.* **37**, 2147–2155
13. Kim, W. S., Hsiao, J. H., Bhatia, S., Glaros, E. N., Don, A. S., Tsuruoka, S., Shannon Weickert, C., and Halliday, G. M. (2013) ABCA8 stimulates sphingomyelin production in oligodendrocytes. *Biochem. J.* **452**, 401–410
14. Chrast, R., Saher, G., Nave, K. A., and Verheijen, M. H. (2011) Lipid metabolism in myelinating glial cells: lessons from human inherited disorders and mouse models. *J. Lipid Res.* **52**, 419–434
15. Dugas, J. C., Tai, Y. C., Speed, T. P., Ngai, J., and Barres, B. A. (2006) Functional genomic analysis of oligodendrocyte differentiation. *J. Neurosci.* **26**, 10967–10983
16. HD iPSC Consortium. (2012) Induced pluripotent stem cells from patients with Huntington's disease show CAG-repeat-expansion-associated phenotypes. *Cell Stem Cell* **11**, 264–278
17. Bleasel, J. M., Hsiao, J. H., Halliday, G. M., and Kim, W. S. (2013) Increased expression of ABCA8 in multiple system atrophy brain is associated with changes in pathogenic proteins. *J. Parkinsons Dis.* **3**, 331–339
18. Mirza, N., Vasieva, O., Marson, A. G., and Pirmohamed, M. (2011) Exploring the genomic basis of pharmacoresistance in epilepsy: an integrative analysis of large-scale gene expression profiling studies on brain tissue from epilepsy surgery. *Hum. Mol. Genet.* **20**, 4381–4394
19. Voutetakis, K., Chatziioannou, A., Gonos, E. S., and Trougakos, I. P. (2015) Comparative meta-analysis of transcriptomics data during cellular senescence and in vivo tissue ageing. *Oxid. Med. Cell Longev.* **2015**, 732914
20. Liu, H., Yang, Y., Xia, Y., Zhu, W., Leak, R. K., Wei, Z., Wang, J., and Hu, X. (2017) Aging of cerebral white matter. *Ageing Res. Rev.* **34**, 64–76
21. Rosas, H. D., Wilkens, P., Salat, D. H., Mercaldo, N. D., Vangel, M., Yendiki, A. Y., and Hersch, S. M. (2018) Complex spatial and temporally defined myelin and axonal degeneration in Huntington disease. *Neuroimage Clin.* **20**, 236–242
22. Faber, J., Giordano, I., Jiang, X., Kindler, C., Spottke, A., Acosta-Cabronero, J., Nestor, P. J., Machts, J., Düzel, E., Vielhaber, S., Speck, O., Dudesek, A., Kamm, C., Scheef, L., and Klockgether, T. (2020) Prominent white matter involvement in multiple system atrophy of cerebellar type. *Mov. Disord.* **35**, 816–824
23. Rodríguez-Cruces, R., and Concha, L. (2015) White matter in temporal lobe epilepsy: clinico-pathological correlates of water diffusion abnormalities. *Quant. Imaging Med. Surg.* **5**, 264–278
24. Wong, J. H., Halliday, G. M., and Kim, W. S. (2014) Exploring myelin dysfunction in multiple system atrophy. *Exp. Neurol.* **23**, 337–344
25. Wertman, V., Gromova, A., La Spada, A. R., and Cortes, C. J. (2019) Low-cost gait analysis for behavioral phenotyping of mouse models of neuromuscular disease. *J. Vis. Exp.* <https://doi.org/10.3791/59878>
26. Chojnowski, A., Ong, P. F., Wong, E. S., Lim, J. S., Mutalif, R. A., Navasankari, R., Dutta, B., Yang, H., Liow, Y. Y., Sze, S. K., Boudier, T., Wright, G. D., Colman, A., Burke, B., Stewart, C. L., *et al.* (2015) Progerin reduces LAP2 α -telomere association in Hutchinson-Gilford progeria. *Elife* **4**, e07759
27. Shevchenko, A., Tomas, H., Havlis, J., Olsen, J. V., and Mann, M. (2006) In-gel digestion for mass spectrometric characterization of proteins and proteomes. *Nat. Protoc.* **1**, 2856–2860
28. Arganda-Carreras, I., Fernández-González, R., Muñoz-Barrutia, A., and Ortiz-De-Solorzano, C. (2010) 3D reconstruction of histological sections: application to mammary gland tissue. *Microsc. Res. Tech.* **73**, 1019–1029
29. Stauffer, W., Sheng, H., and Lim, H. N. (2018) EzColocalization: an ImageJ plugin for visualizing and measuring colocalization in cells and organisms. *Sci. Rep.* **8**, 15764
30. Bronzert, T. J., and Brewer, H. B., Jr. (1977) New micromethod for measuring cholesterol in plasma lipoprotein fractions. *Clin. Chem.* **23**, 2089–2098
31. Alshehry, Z. H., Barlow, C. K., Weir, J. M., Zhou, Y., McConville, M. J., and Meikle, P. J. (2015) An efficient single phase method for the extraction of plasma lipids. *Metabolites* **5**, 389–403
32. Tachikawa, M., Toki, H., Watanabe, M., Tomi, M., Hosoya, K.-I., and Terasaki, T. (2018) Gene expression of A6-like subgroup of ATP-binding cassette transporters in mouse brain parenchyma and microvessels. *Anat. Sci. Int.* **93**, 456–463
33. Annilo, T., Chen, Z.-Q., Shulenin, S., and Dean, M. (2003) Evolutionary analysis of a cluster of ATP-binding cassette (ABC) genes. *Mamm. Genome* **14**, 7–20
34. Zhang, Y., Chen, K., Sloan, S. A., Bennett, M. L., Scholze, A. R., O'Keefe, S., Phatnani, H. P., Guarnieri, P., Caneda, C., Ruderisch, N., Deng, S., Liddelow, S. A., Zhang, C., Daneman, R., Maniatis, T., *et al.* (2014) An RNA-sequencing transcriptome and splicing database of glia, neurons, and vascular cells of the cerebral cortex. *J. Neurosci.* **34**, 11929–11947
35. Novak, G., Fan, T., O'Dowd, B. F., and George, S. R. (2013) Striatal development involves a switch in gene expression networks, followed by a myelination event: implications for neuropsychiatric disease. *Synapse* **67**, 179–188
36. Mikoshiba, K., Okano, H., Tamura, T., and Ikenaka, K. (1991) Structure and function of myelin protein genes. *Annu. Rev. Neurosci.* **14**, 201–217
37. Li, Z., Fan, Y., Liu, J., Li, Y., Huan, C., Bui, H. H., Kuo, M. S., Park, T. S., Cao, G., and Jiang, X. C. (2012) Impact of sphingomyelin synthase 1 deficiency on sphingolipid metabolism and atherosclerosis in mice. *Arterioscler. Thromb. Vasc. Biol.* **32**, 1577–1584
38. Girolamo, F., Ferrara, G., Strippoli, M., Rizzi, M., Errede, M., Trojano, M., Perris, R., Roncali, L., Svelto, M., Mennini, T., and Virgintino, D. (2011) Cerebral cortex demyelination and oligodendrocyte precursor response to experimental autoimmune encephalomyelitis. *Neurobiol. Dis.* **43**, 678–689
39. Fink, A. J., Englund, C., Daza, R. A., Pham, D., Lau, C., Nivison, M., Kowalczyk, T., and Hevner, R. F. (2006) Development of the deep cerebellar nuclei: transcription factors and cell migration from the rhombic lip. *J. Neurosci.* **26**, 3066–3076
40. Kucharova, K., and Stallcup, W. B. (2010) The NG2 proteoglycan promotes oligodendrocyte progenitor proliferation and developmental myelination. *Neuroscience* **166**, 185–194
41. Kuhn, S., Gritti, L., Crooks, D., and Dombrowski, Y. (2019) Oligodendrocytes in development, myelin generation and beyond. *Cells* **8**, 1424
42. Tansey, F. A., and Cammer, W. P. (1991) A pi form of glutathione-S-transferase is a myelin- and oligodendrocyte-associated enzyme in mouse brain. *J. Neurochem.* **57**, 95–102
43. Roux, K. J., Kim, D. I., Raida, M., and Burke, B. (2012) A promiscuous biotin ligase fusion protein identifies proximal and interacting proteins in mammalian cells. *J. Cell Biol.* **196**, 801–810
44. Sakry, D., and Trotter, J. (2016) The role of the NG2 proteoglycan in OPC and CNS network function. *Brain Res.* **1638**, 161–166
45. de Vrij, F. M., Bouwkamp, C. G., Gunhanlar, N., Shpak, G., Lendemeijer, B., Baghdadi, M., Gopalakrishna, S., Ghazvini, M., Li, T. M., Quadri, M., Olgiati, S., Breedveld, G. J., Coesmans, M., Mientjes, E., de Wit, T., *et al.* (2019) Candidate CSPG4 mutations and induced pluripotent stem cell modeling implicate oligodendrocyte progenitor cell dysfunction in familial schizophrenia. *Mol. Psychiatry* **24**, 757–771
46. Reynolds, R., and Wilkin, G. P. (1988) Development of macroglial cells in rat cerebellum. II. An in situ immunohistochemical study of oligodendroglial lineage from precursor to mature myelinating cell. *Development* **102**, 409–425
47. Lee, P. R., and Fields, R. D. (2009) Regulation of myelin genes implicated in psychiatric disorders by functional activity in axons. *Front. Neuroanat.* **3**, 4
48. Rushton, W. A. H. (1951) A theory of the effects of fibre size in medullated nerve. *J. Physiol.* **115**, 101–122
49. Chambers, W. W., and Sprague, J. M. (1955) Functional localization in the cerebellum I: organization in longitudinal corticocortical zones and their contribution to the control of posture, both extrapyramidal and pyramidal. *J. Comp. Neurol.* **103**, 105–130
50. Voineskos, A. N., Lobaugh, N. J., Bouix, S., Rajji, T. K., Miranda, D., Kennedy, J. L., Mulsant, B. H., Pollock, B. G., and Shenton, M. E. (2010) Diffusion tensor tractography findings in schizophrenia across the adult lifespan. *Brain* **133**, 1494–1504
51. Yang, J., Price, M. A., Wanshura, L., He, J., Yi, M., Welch, D. R., Li, G., Conner, S., Sachs, J., Turley, E. A., and McCarthy,

- J. B. (2019) Chondroitin sulfate proteoglycan 4 enhanced melanoma motility and growth requires a cysteine in the core protein transmembrane domain. *Melanoma Res.* **29**, 365–375
52. Quarles, R. H., Macklin, W. B., and Morell, P. (2006) Myelin formation, structure and biochemistry. In *Basic Neurochemistry: Molecular, Cellular and Medical Aspects*, 7th Ed, G. J. Siegel, B. W. Agranoff, R. W. Albers, S. K. Fisher, and M. D. Uhler, editors. Lippincott-Raven, Philadelphia, 51–71
53. Braverman, N. E., and Moser, A. B. (2012) Functions of plasmalogen lipids in health and disease. *Biochim. Biophys. Acta.* **1822**, 1442–1452
54. Bams-Mengerink, A. M., Majoie, C. B., Duran, M., Wanders, R. J., Van Hove, J., Scheurer, C. D., Barth, P. G., and Poll-The, B. T. (2006) MRI of the brain and cervical spinal cord in rhizomelic chondrodysplasia punctata. *Neurology.* **66**, 798–803
55. Teigler, A., Komljenovic, D., Draguhn, A., Gorgas, K., and Just, W. W. (2009) Defects in myelination, paranode organization and Purkinje cell innervation in the ether lipid-deficient mouse cerebellum. *Hum. Mol. Genet.* **18**, 1897–1908
56. von Boxberg, Y., Soares, S., Féréol, S., Fodil, R., Bartolami, S., Taxi, J., Tricaud, N., and Nothias, F. (2014) Giant scaffolding protein AHNAK1 interacts with β -dystroglycan and controls motility and mechanical properties of Schwann cells. *Glia.* **62**, 1392–1406
57. Manavalan, A., Mishra, M., Feng, L., Sze, S. K., Akatsu, H., and Heese, K. (2013) Brain site-specific proteome changes in aging-related dementia. *Exp. Mol. Med.* **45**, e39
58. Mez, J., Chung, J., Jun, G., Kriegel, J., Bourlas, A. P., Sherva, R., Logue, M. W., Barnes, L. L., Bennett, D. A., Buxbaum, J. D., Byrd, G. S., Crane, P. K., Ertekin-Taner, N., Evans, D., Fallin, M. D., *et al* (2017) Two novel loci, COBL and SLC10A2, for Alzheimer's disease in African Americans. *Alzheimers Dement.* **13**, 119–129
59. Nasrabad, S. E., Rizvi, B., Goldman, J. E., and Brickman, A. M. (2018) White matter changes in Alzheimer's disease: a focus on myelin and oligodendrocytes. *Acta Neuropathol. Commun.* **6**, 22